# Multiple-scale Simulation Method for Liquid with Trapped Air under Particle-based Framework

Sinuo Liu* Ben Wang† Xiaojuan Ban‡

Beijing Advanced Innovation Center for Materials Genome Engineering,
School of computer and communication Engineering,
University of Science and Technology Beijing

**ABSTRACT**

Trapped air in liquid is an important factor which affect the realism of fluid simulation. However, due to the complex physical properties, simulating the interaction and transformation between air and liquid is extremely challenging and time-consuming. In this paper, we propose a multi-scale simulation method under particle-based framework to achieve the realistic and efficient simulation of air-liquid fluid. A unified generation rule is proposed according to the kinetic energy and the velocity difference between fluid particles. Two velocity-based dynamic models are then established for different size of air materials respectively. The Brownian motion of small scale air materials is achieved by Schilk random function. The interaction and air transfer between large scale air materials is achieved by inverse diffusion equation and a new high-order kernel function. Experimental results show that the proposed method can improve the fidelity and richness of the fluid simulation. The post-processing scheme makes it able to be integrated with existing particle method easily.

**Index Terms:** Computing methodologies—Computer graphics—Animation—Physical simulation

## 1 INTRODUCTION

Existing fluid simulation methods, including particle-based methods and grid-based method, is able to describe the macroscopic motion trend of the fluid realistically [3, 8, 37], which puts higher requirements on the detail simulation, such as foam and bubbles [4, 17]. Liquid with trapped air is essentially a mixture of a large amount of liquid and a small amount of air. Due to nucleation [9, 31], trapped air [18, 30], and boiling [21, 29], air materials with different physical properties are generated in fluid. Without these air materials, the realism of fluid animation will decreased significantly. However, the physical laws of the generation, interactions, dissipation and mass transfer are extremely complex. This make it difficult to simulate air materials in fluid realistically.

The study of air-liquid fluid is mainly divided into two types according to their size. When modeling of the large-size air materials [1, 21], the fluid is usually regarded as a air-liquid two-phase fluid, and a complex physical model will be established including buoyancy force and drag force. This type of models are able to describe the shape change of bubbles vividly, but the calculation process is extremely time consuming [15]. Besides, the phenomenon of mass transfer between bubbles cannot be well described.

As for the simulation of the small size air materials, the shape and size of the particles is usually ignored, and only the macroscopic motion trend is described [14]. Generally, this type of model is a post-processing model which can enhance visual effects with negligible computational overhead. However, it usually focuses on only the free surface. Since most details are lost, its advantages can only be achieved when shooting from a long distance. Besides, if Brownian motion is not considered, large number of air particles will move with similar motion patterns, which result in a extremely regular periodic distribution and affect the visual effect [18]. In real life, air bubbles of different sizes (like large bubbles and small foams) are usually generated at the same time. Simulating different scales of air materials simultaneously in a unified framework can achieve a more realistic results.

In order to combine the advantages of the above two methods, we propose a unified multiple-scale air material simulation method for particle-based fluid. In this paper, areas where entrapped air are determined by the kinetic energy and velocity difference of fluid particles. air materials are divided into six different types depending on the size and coupling degree with the fluid, and different dynamic models are designed separately. By ignoring the feedback of small-mass air particles on large-mass fluid particles, efficient one-way coupling is achieved through the velocity field, which greatly improves the calculation efficiency. The Brownian motion of air materials is simulated using a random emitter. The interaction between the air particles is described by a new high-order kernel function based on Lennard-Jones function to ensure their stable status conforms to Plateau equilibrium distance. An inverse diffusion equation was introduced to describe the air transfer between two large-scale air particles. The main contributions of this paper are as follows:

- A multiple-scale air material simulation method under unified particle-based framework, with adjustable control parameters to achieve different visual effect.
- A new dynamics model for large-size air material, including air transfer model based on the inverse diffusion equation, and interaction scheme using a new high-order kernel function.
- A new dynamics model based on Schilk random function for small-size air material, which solve the problem of regular distribution of air particles by implementing Brownian motion.

## 2 RELATED WORK

Fluid simulation is an important research topic in computer graphics. With the development of the entertainment industry and Virtual Reality, the demand for fluid simulation is increasing [38, 39]. For better understanding of the whole research area, we recommend the groundbreaking work of Stam [32] and the book of Bridson [6]. In this section, we discuss related work on fluid simulation (section 2.1) and air materials simulation (section 2.2).

### 2.1 Fluid Simulation

Fluid motion can be described in two forms: Euler description based on the spatial point of the flow field and Lagrangian description based on the fluid particle. Therefore, fluid simulation methods

*e-mail: liusinuo@xs.ustb.edu.cn
†e-mail: ben_ben_wang@yeah.net
‡Corresponding author, e-mail: banxj@ustb.edu.cn

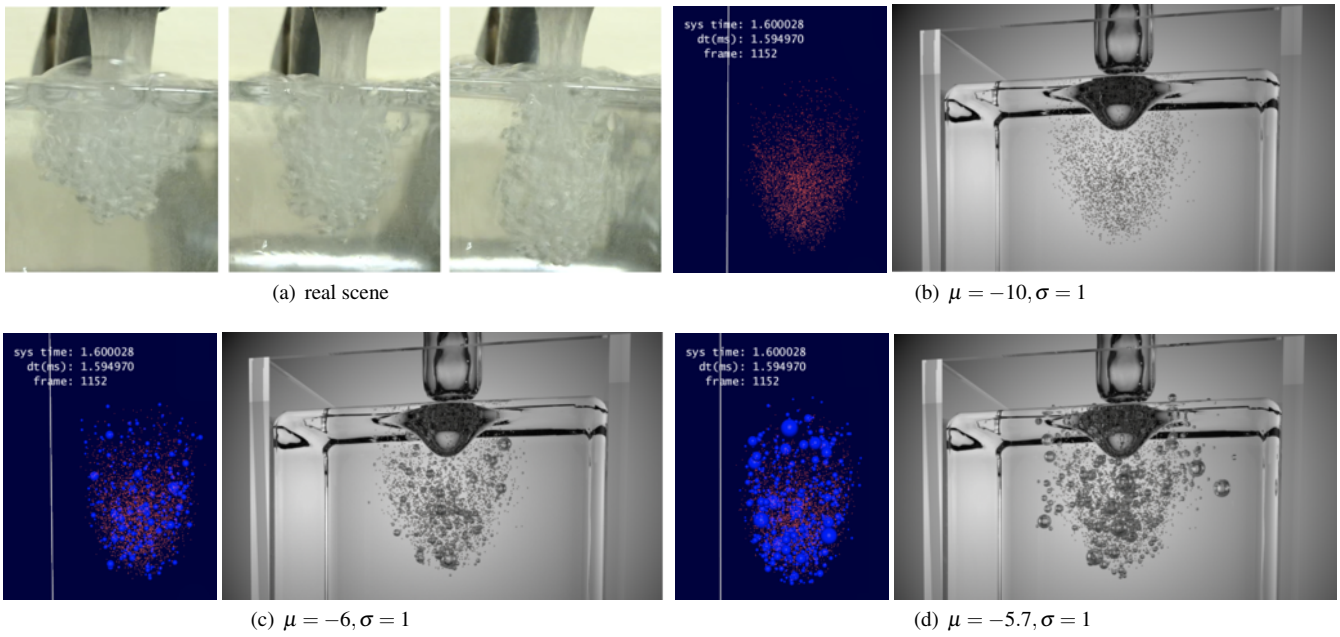


(a) real scene (b) $\mu = -10, \sigma = 1$

(c) $\mu = -6, \sigma = 1$ (d) $\mu = -5.7, \sigma = 1$

Figure 1: Injecting water into a pool with 29k fluid particles. (a) is the real scene, (b)(c)(d) are the simulation results with particle result on the left and rendered result on the right. In particle result, small size air materials and large size air materials are marked as red dot and blue sphere, respectively. By adjusting control parameter $\mu$ in Eq.5, the occupation of large air particle is changed, and different styles are realized. The proportion of large-sized particles in (b)(c) and (d) is 0%, 8.23% and 13.80%, respectively. The visual effect in (d) is more similar to real scene.

are also divided into two categories: grid-based Euler method and particle-based Lagrangian method [34]. Both methods are based on the fluid's control equations but differ in discretization process. Since the discretization is more regular, it is easy for grid method to derive simple formulas that are easy to calculate. However, due to the limitations of fixed grid points, its spatial flexibility is not as good as particle-based method. For intense or complex scenes, particle-based method is able to capture details better.

Air-liquid fluids are usually generated in highly deformed fluids. Therefore, the Lagrange-based method is very suitable for simulating scenes containing air materials. In this paper, we use a classical particel-based method, Smoothed Particle Hydrodynamics (SPH method) [26] for fluid simulation. For the latest development, we would like to refer to two reviews [20] and [15].

## 2.2 Air Material Simulation

In terms of air-liquid fluid simulation, it can be divided into three categories according to the generating mechanism: trapped air(section 2.2.1), nucleation and boiling(section 2.2.2). Our method is illustrated in section 2.2.3.

### 2.2.1 Trapped Air

When moving intensely or rushing quickly, air will be trapped in fluid. This type of air materials are usually divided into two categories according to their size, and the simulation mechanisms are also different.

**Large Size Air Materials.** Many researches focus on the coupling of air-liquid two-phase flow. Air materials, such as bubbles and foam, are considered as air phase and be simulated as macroscopic air bubbles in fluids [10].

In 2005, Muller et al. [27] proposed a bubble generation rule based on the color field, which can generate bubble particles in the SPH multi-phase flow solver dynamically. Hong et al. [13] used the SPH method to simulate non-deformable bubbles, and used a level set method to simulate deformable bubbles and fluids. Air and liquid are coupled through a velocity field. However, due to the limitation of the grid resolution, this method is difficult to simulate the unstable motion when bubbles rising. Akinci et al. [1] separately processed the air-liquid two phases, calculated the density and pressure of the two phases using SPH method, and simulated the interaction of the two phases through the velocity field. This method solves the problem of high density ratio and can simulate complex bubble motion in water. However, since the SPH method must ensure a certain initial particle spacing, the number of bubble particles is limited by the resolution of the fluid particles. In 2012, Busaryev et al. [7] proposed an algorithm to simulate bubbles in dense foam. By applying strong interactions, the arrangement and geometry of bubbles are more in line with physics laws. Ren et al. [30] used volume fraction representation to simulate various bubble effects in multiphase flow simulations. The deformation and dissolution of bubbles, and accumulation of foams can be handled simultaneously.

**Small Size Air Material.** Some research ignored the effect of air phase to the liquid phase, to avoid the excessive calculation cost in multiphase flow model.

Takahashi et al. [33] combined a grid-based fluid solver (Constrained Interpolation Profile, CIP method) with a particle-based air material solver and proposed a splash and foam simulation method. Air particles are added at area with larger curvatures over free surface. In 2007, Thürey et al. [35] proposed a bubble and foam simulation method based on shallow water equations. This method can simulate scene with millions of air particles, but the simplified equation makes it difficult to describe the interaction of the fluid. Onderik et al. [28] used particle emitter to simulate waves in the ocean. Bubble particles concentrated on the peaks of the waves can be modeled realistically. In order to speed up the simulation, the interaction between bubble particles is ignored. Inspired by the work of Onderik [28] and Takahashi [33], Ihmsen et al. [14] proposed to simulate the air materials (bubble, foam, and spray) in the waves using a unified particle system. Through a post-processing velocity-based coupling, the motion of the air materials can be efficiently simulated. However,

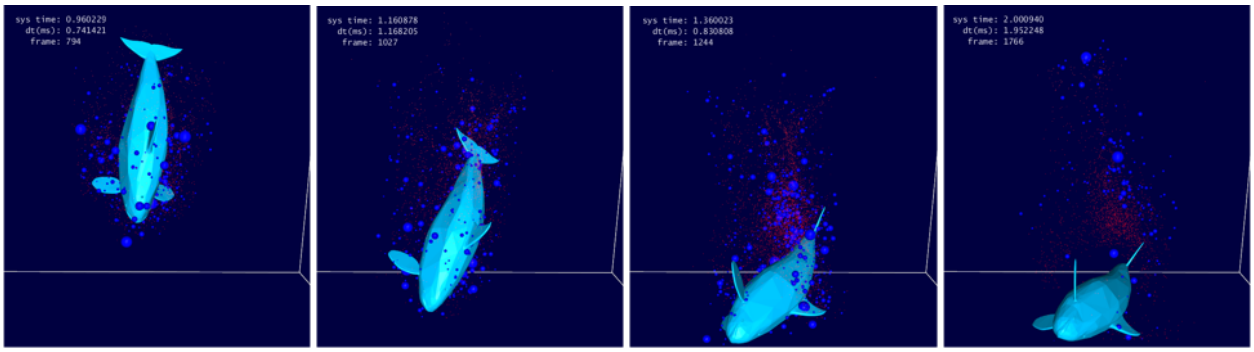


(a) particle result of air materials and solid body

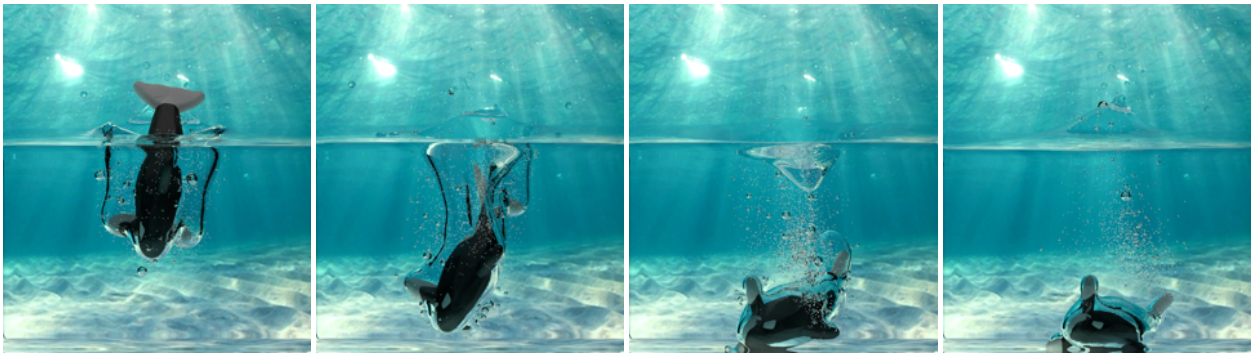

(b) rendered result

Figure 2: Experiment of a dolphin diving in the sea with 76k particles. To show the status of air materials more clearly, the particle results with a rigid body are shown in (a). Among them, small size air materials and large air materials are represented by red dots and blue spheres, respectively. In this experiment, dolphin interact with fluids and create disturbances, forming air materials in varying sizes. As can be seen in the last two columns, when the dolphin swings its caudal fin, air material has a tendency to follow.

due to insufficient randomness, the generated air materials exhibit a relatively regular distribution, resulting in an unrealistic visual effect. In the real world, each rising bubble will produce a wake that affects the motion of itself and neighbor bubbles. Due to the influence of the wake, the motion state and spatial distribution of the air materials are very irregular [12, 16]. However, to ensure the stability of the simulation, the properties of each fluid particle will be smoothed by the information of neighbor fluid particles. Physical properties such as velocity and acceleration of spatially adjacent fluid particles are extremely similar. Since the support area of the air particles is constant during the simulation, the spatially adjacent air particles have substantially the same fluid neighbors, and the velocity update values are also very similar (see Fig. 3). To solve this problem, Kim et al. [18] proposed an efficient foam simulation method by incorporating projective space. However, as a screen space-based technique, this method can only generate foam particles in view-dependent areas, which means air materials may failed to be generated in regions occluded by an object.

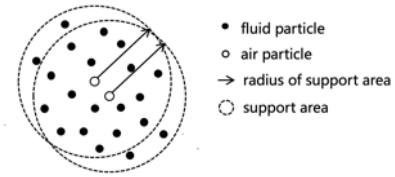


Figure 3: Spatially adjacent air particles have substantially the same neighbor fluid particles. The motion of air particles depends to a large extent on the average velocity of its neighboring fluid particles $\hat{\mathbf{v}}_f$ (see Eq. 9). Therefore, if Brownian motion is not added, regular periodic distribution of air materials will be observed (see Fig.5(b)).

### 2.2.2 Nucleation and Boiling

**Nucleation.** When environmental conditions such as temperature, pressure, and impurities change, air originally dissolved in water may precipitate to generate nucleating bubbles (e.g. foam in beer). At present, there are few studies on nucleation phenomena in the field of computer animation. Cleary et al. [9] used the diffusion equation of air to simulate nucleation bubbles generated by air dissolution. Bubbles are modeled by discrete spherical with fixed shapes. The coupling between air materials and liquid is achieved by drag forces, and the effect of the air materials on the liquid is ignored. Shao et al. [31] proposed a new generation model of air materials by taking into account the air concentration and the liquid-solid velocity difference. When the air particles on the bubble surface are regarded as virtual nucleation point, this bubbles will absorb air from the surrounding liquid and grow big.

**Boiling.** Boiling is a phenomenon in which the free surface and inside liquid vaporizes simultaneously when the liquid is heated above its saturation temperature. Kim and Carlson [19] considered the boiling process as a independent module. By using Yanagita boiling model, only the thermal field is operated, and do not need to track the pressure, viscosity and free surface accurately. Mihalef et al. [23] added temperature field and mass transfer mechanism based on the CLSVOF two-phase flow model. The experimental results shows the subtle effects of the cycle on bubble motion. Their algorithms remain stable as the topology changes. Prakash et al. [29] proposed a SPH-based boiling method using the local superheat

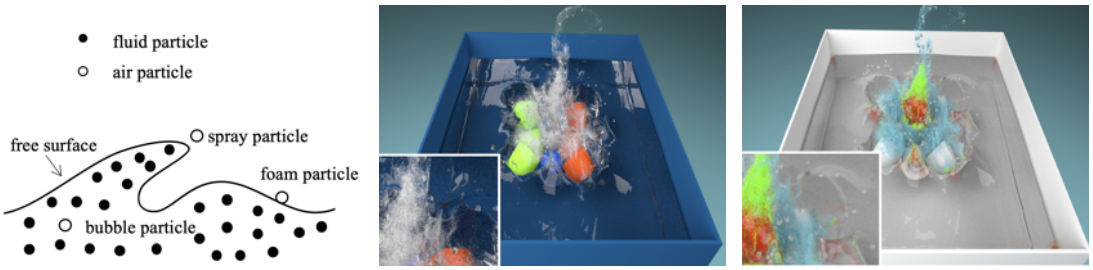


(a) classification rule (b) rendered result (c) marked result

Figure 4: Both large size and small size air particle are classified by the coupling degree with fluid (see section 3.3). Subfigure (b) shows the render result of air materials generated by stuffs falling into water. The marked result is shown in the subfigure (c), where spray particle, foam particle, bubble particle are marked by lighr blue, green and red, redpectively.

of the fluid, with adjustable key parameters to design the boiling process. The work of Gu et al. [11] deals with vapor particles rather than air particles, allowing the bubbles to recondense into a liquid during exercise. Li et al. [21] proposed a boiling model based on the PBF fluid solver, considering the effects of heat conduction and thermal convection on the boiling process.

#### 2.2.3 Our Method

Our method is a multicle-scale air-liquid fluid simulation method, which consider the air materials as generated by trapped air. The size of air particle is determined by a random function. The dynamics model of large size air particles and small size air particles are designed separately. The coupling between of air particles and fluid is achieved via velocity field by post-process step. The interaction between large size air particles is modeled using a new high-order kernel function based on Lennard-Jones function. The Brownian motion of small air particles and the air transfer between large air particles are also achieved in this paper.

## 3 Generation and Deletion of air Materials

The generation scheme is inspired by paper [14] but different slightly. Previous methods tend to generate air particles at free surfaces with large curvatures, but we found the visual effect of this part of the air materials is not that obvious, and the calculation process is complicated. Therefore, we do not consider curvatures, only control the generation of foam based on the velocity difference and kinetic energy. Due to the small supporting radius and the small moving distance of the fluid particle in each time step, air particles tend to form a cluster under this initialization scheme. To solve the problem, we set the size of the generation area(cylinder) to be adjustable(more larger), and a more realistic results could be obtained. The air particles are divided into six types based on the size and coupling degree with fluid. Deletion is achieved using a Probability function.

### 3.1 Generation of Air Particles

Air materials in the flow field are usually generated in areas with high-speed and complex motion. With larger kinetic energy and higher disorder degree, more air material will be generated. For each fluid particle $i$ , the quantity of air particles $Q_i^k$ and $Q_i^v$ generated is related to the kinetic energy and velocity difference:

$$Q_i^k = \sum_j \frac{1}{2} m_i \mathbf{v}_i^2 \qquad Q_i^v = \lambda \|\mathbf{v}_{ij}\| \cdot W_{ij}^Q \tag{1}$$

where $j$ is used to iterate neighboring fluid particles, $\lambda = 1 - \frac{\mathbf{x}_{ij}}{\|\mathbf{x}_{ij}\|} \cdot \frac{\mathbf{v}_{ij}}{\|\mathbf{v}_{ij}\|}$ is used to determine the relative movement of particles, $\mathbf{x}_{ij} = \mathbf{x}_i - \mathbf{x}_j$ and $\mathbf{v}_{ij} = \mathbf{v}_i - \mathbf{v}_j$ are the position difference vector and velocity difference vector of particle $i$ and $j$. When $\lambda > 0$, particles are moving towards each other in opposite directions, and vice versa. $W_{ij}^Q = W^Q(\mathbf{x}_{ij}, h)$ is a normalized kernel function with $W_{ij}^Q = 1 - \frac{\|\mathbf{x}_{ij}\|}{r}$ if $\|\mathbf{x}_{ij}\| < r$, and euqals to zero in other case, where $r$ is the radius of the support area.

The quantity of air material generated by each fluid particle is then mapped to [0,1] with $R_i = \frac{Q_{max} - Q_i}{Q_{max} - Q_{min}}$ if $Q_{min} < Q_i \leq Q_{max}$. $R_i = 0$ when $Q_i \leq Q_{min}$, and $R_i = 1$ when $Q_{max} \leq Q_i$, where $Q_{max}$ and $Q_{min}$ are user-defined parameters represent the maximum and minimum values respectively. So we have four parameters ($Q_{max}^k$, $Q_{min}^k$, $Q_{max}^v$, $Q_{min}^v$) and two air particle generation rates ($R_i^k$ and $R_i^v$) here. When $R_i^k \cdot R_i^v$ is greater than zero, the fluid particles are selected as candidate particles and $n_a$ air particles are generated nearby:

$$n_a = R_i^k \cdot R_i^v \cdot n_{max} \cdot \delta t \tag{2}$$

where $n_{max}$ is the maximum sampling rate.

In each time-step, fluid particles move along $\mathbf{x}(t)$ and $\mathbf{x}(t + \delta t)$. $n_a$ air particles are randomly generated in a cylinder centered on this connecting line. Its bottom radius is set by a random variable and the support radius $r$ . Two linearly independent vectors $\vec{n}_1$ and $\vec{n}_2$ which are perpendicular to vector $\delta \mathbf{x}_f$ is chosen randomly. The relative position of the air particle $d$ in the cylinder is determined by $h_a = k_h \|\mathbf{x}(t + \delta t) - \mathbf{x}(t)\|$, $\theta_a = k_\theta \cdot 2\pi$, and $r_a = k_r \cdot r$, where $h_a$ is the height of the air particles in the cylinder, $\theta_a$ is the azimuth, $r_a$ is the distance from the center axis of the cylinder. $k_h$, $k_r$, $k_\theta$ are random parameters, and particles are generated outside with the random parameter larger than 1. According to coordinate transform and base conversion, the velocity and position of the air particles in the flow field is obtained:

$$\mathbf{v}_a(t + \delta t) = r_a \cdot cos\theta_a \cdot \vec{n}_1 + r_a \cdot sin\theta_a \cdot \vec{n}_2 + \mathbf{v}_f \tag{3}$$

$$\mathbf{x}_a(t + \delta t) = \mathbf{x}_f(t) + r_a \cdot cos\theta_a \cdot \vec{n}_1 + r_a \cdot sin\theta_a \cdot \vec{n}_2 + h_a \cdot \mathbf{v}_f \tag{4}$$

### 3.2 Multiple-scale Classification of Air Particles

According to the radius, air particles are divided into two categories: small-size air materials and large-size air materials. In physics, bubble radius in the liquid obeys a lognormal distribution [22]. A random number obeying a lognormal distribution is used to determine the initial radius $radius_a$ of a air particle. The probability density function of the lognormal distribution is as follows:

$$p(radius_a) = \begin{cases} \frac{1}{radius_a \sigma \sqrt{2\pi}} e^{-\frac{(\ln x - \mu)^2}{2\sigma^2}}, & radius_a > 0 \\ 0, & radius_a \leq 0 \end{cases} \tag{5}$$

where the probability density function parameters $\sigma$ and $\mu$ is adjustable. Mathematical expectations $E(radius_a)$ and variances

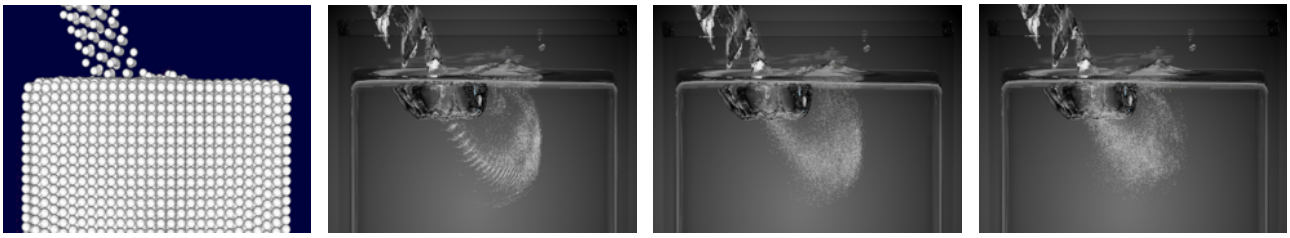

(a) particle result (b) render result with $\kappa = 1$ (c) render result with $\kappa = 0.8$ (d) render result with $\kappa = 0.6$

Figure 5: Tilt water injection (20k particles). In order to see the effect of Brownian motion more clearly, only the small size air particel is rendered. By adjusting the Brownian coefficient $\kappa$, the motion freedom degree of air material changes. The value of $\kappa$ in subfigure (b), (c) and (d) is 1, 0.8, 0.6, respectively. When $\kappa = 1$ (see Fig.5(b)), Brownian motion is not added, and the distribution of the air material is periodic. After adding Brownian motion, the visual effect is improved. We found $\kappa = 0.8$ gives the best result, and all the other experiment use this value.

Table 1: The six types of air particles. The size (large, small) is classified by Eq. 5, the coupling degree with fluid (high, middle, low) is classified by the number of fluid neighbors.

| | **High-coupling** | **Middle-coupling** | **Low-coupling** |
|---|---|---|---|
| **Large-size** | large bubble | large foam | large spray |
| **Small-size** | small bubble | small foam | small spray |

$D(radius_a)$ are:

$$E(radius_a) = e^{\mu + \frac{\sigma^2}{2}} \tag{6}$$

$$D(radius_a) = (e^{\sigma^2} - 1)e^{2\mu + \sigma^2} \tag{7}$$

In addition, a controllable parameter $r_{size} = 0.01m$ is introduced as a threshold for dividing the size of the air material (see Fig. 6). When $radius_a > r_{size}$, the air particles are regarded as large-size air material. When $radius_a \leq r_{size}$, the air particles are regarded as small-size air material, and their radii are valued as the mathematical expectations $E(radius_a)$.

Air particles are affected by gravity, buoyancy, and fluid drag force during movement. The value of the force depends on the degree of coupling with liquid. According to the number of fluid neighbor, air particles are divided into three categories (see Fig. 4): spray, foam and bubbles. Spray particles have less than six fluid neighbors, foam particles have six to twenty neighbors, and bubble particles have more than twenty neighbors. Therefore, there are 6 kinds of air materials in this paper, as shown in Table 1.

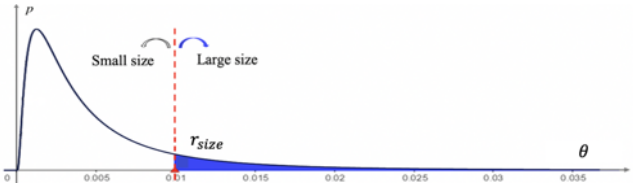


Figure 6: The classication rule of air particle size. A adjustable paremeter $\theta$ is used to determined the category of all air particles. Each larger one will be regarded as large size air particle with a random radius. Each smaller one will be regarded as a small size air particle with a unified radius calculated by Eq. 6

### 3.3 Deletion of Air Particles

Air particles are dynamic surviving particles. Their stability is affected by many factors, such as the size and the coupling degree with liquid. On one hand, the highly-coupled air particles are relatively stable due to its high liquid proportion. Under gravity, the liquid discharge phenomenon occurs, so that the liquid film between the air materials becomes thinner. The other two coupled types are more likely to be broken. On the other hand, according to the Gibbs principle, a system always tends to a lower surface energy state, so small air particles with lower surface energy are more stable. The surface liquid discharge rate of the large-size air particles is faster, which makes the stability relatively poor.

To simulate the above phenomenon, in each time step, we randomly remove the air particles based on their age and radius. The probability that a air particle $a$ is deleted is:

$$P_i = 1 - (\frac{1}{2})^{\frac{l_a^{age} \cdot radius_a}{T}} \tag{8}$$

where $T$ is the half-life period. Equation 8 shows that and the larger and older air particles are more likely to be deleted.

## 4 Dynamics Models for Air-liquid Fluid Interaction

In this paper, two dynamics models are established for different size of air materials. The small size air particles move under the gravity, the buoyancy and the coupling force with fluid [14], while the large size air particle will also coupling with neighbor air particles and solid particles [1]. We improved the velocity update function for small size foam particles to get a better results (see Fig. 7). Brownian motion of small size bubble particles is achieved by a random function. For the large-size air particles dynamic, it is necessary to search their fluid neighbors, solid neighbors and air neighbors. Then some important microscopic effects, including aggregation, collision and gas transmission process between air materials could be achieved. A new high-order kernel function is used to handle the interaction between large air particles to achieve plateau equilibrium. Mass transfer phenomenon is achieved by using inverse diffusion equation.

Traditional two-way coupling requires cross-neighborhood search. When the fluid motion is intense, the number of air particles increases exponentially, and the time spent on cross-neighborhood search becomes unacceptable. In this paper, the one-way coupling scheme is realized through the velocity field. The feedback form a air particle to a fluid particle is ignored based on the following two reason: a) the mass of the air particles is much smaller than that of the fluid particles; b) this paper does not involve the highly disturbed scene in which air material effect the fluid significantly, e.g. boiling. In addition, the numerical instability of the interactive interface caused by the density fluctuation [27] is avoided.

### 4.1 Small-size Air Particle Dynamics Model

As shown in Fig. 7, in each time step, the velocity of the air particle located at $\mathbf{x}_a$ is calculated together by the velocity variation caused

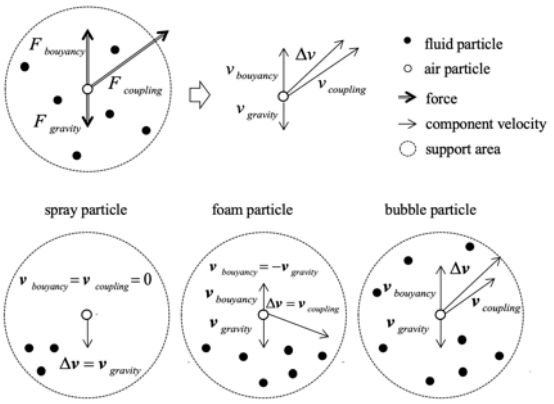


Figure 7: The force analysis for small-size air particle. Each small air particle will move under gravity, buoyancy and coupling force(see Eq. 9). Due to the difference in coupling degree, the specific velocity update of three small size air material are lightly different(see section 4.1 Coupling Paremeter).

by the gravity $\mathbf{v}_{gravity}$, the buoyancy $\mathbf{v}_{buoyancy}$ and the drag force of the neighboring fluid particles $\mathbf{v}_{coupling}$:

$$\begin{aligned}\mathbf{v}_a(t+\delta t) &= \mathbf{v}_a(t)+\mathbf{v}_{gravity}+\mathbf{v}_{buoyancy}+\mathbf{v}_{coupling}\\ &= \mathbf{v}_a(t)+\mathbf{g}\cdot\delta t+k_a\cdot(-\mathbf{g})\cdot\delta t+k_{cp}\cdot(\hat{\mathbf{v}}_f(t+\delta t)-\mathbf{v}_a(t))\end{aligned} \tag{9}$$

where $\mathbf{g}$ is the gravitational acceleration, $k_b \geq 0$ is the buoyancy parameter, $k_{cp} \in [0,1]$ is the coupling parameter, $\hat{\mathbf{v}}_f = \frac{\sum_f \mathbf{v}_f(t+\delta t)\cdot W_{df}}{\sum_f W_{df}}$ is the average velocity of the neighboring fluid particles, $W_{df}$ is a smooth kernal represented by a b-spline function [25]. $k_b$ and $k_{cp}$ are coupling parameters related to the degree of coupling.

Coupling Parameter. The value of the coupling parameter depends on the degree of coupling. The spray particles are free particles that move along the parabola under the influence of gravity. Their trajectories are not affected by neighboring fluid particles. For spray particles, $k_b^{spray} = k_{cp}^{spray} = 0$.Foam particles float on the free surface and are balanced by gravity and buoyancy, that is $k_b^{foam} = 1$. They are only affected by the drag force of the neighboring fluid particles. Bubble particles interact with the fluid most closely, that is $k_{cp}^{bubble} > k_{cp}^{foam}$, and its motion is also more complicated. Bubble particles are not only affected by the drag force of the neighboring fluid particle, but also rises slowly due to the buoyancy.

Brownian Motion. To produce a more realistic random motion effect, the Schlick Function [5] is used to describe the velocity offset angle $\theta_{BM}$ of each small size bubble particles (see Fig, 8):

$$\theta_{BM} = \arccos\frac{2\zeta+\kappa-1}{2\kappa\zeta-\kappa+1} \tag{10}$$

where $\zeta \in [0,1]$ is a uniform random number, $\kappa \in [-1,1]$ is the Brownian coefficient. When $\kappa < 0$, air particles are diverged in the opposite direction. When $\kappa = 0$, air particles move isotropically. When $\kappa > 0$, air particles diverge forward. Especially when $\kappa = 1$, the diverges effect is not added.

The $Probability_a$ of a air particle $d$ to move following the Brownian Motion is determined by the degree of chaos of this area. In this paper, the linked list neighbor search algorithm [24] is used to store the neighbor fluid particles of air particles in the bucket linked list, The first fluid particle $f_{first}$ in each linked list could be obtained without additional calculation overhead. Since the fluid particles

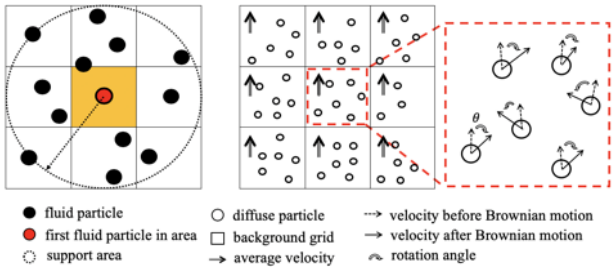


Figure 8: The Brownian motion of small bubble particles.

with similar positions have substantially the same attribute value, $f_{first}$ is selected to calculate the degree of chaos in the region:

$$Probability_a = \left(\frac{R^k_{f_{first}} + R^v_{f_{first}}}{2}\right)^{\frac{1}{4}} \tag{11}$$

### 4.2 Large-size Air Particle Dynamics Model

Due to the large volume of large-size air materials, their coupling degree with the rigid body and the neighboring air material is relatively high. Therefore, in addition to gravity $\mathbf{F}_{gravity} = m_a \cdot \mathbf{g}$, and coupling force with fluid $\mathbf{F}_{Fluid}$, the interaction with the rigid body $\mathbf{F}_{Solid}$ and the air material $\mathbf{F}_{air}$ also needs to be described. The resultant force applied to a large-size air particle $a$ is calculated by the following formula:

$$\mathbf{F}_a = \mathbf{F}_{gravity} + \mathbf{F}_{Fluid} + \mathbf{F}_{Solid} + \mathbf{F}_{air} \tag{12}$$

Coupling with Fluid. Similar to small size air particles, the force between large-size air particle and fluid particle is buoyancy $\mathbf{F}_{buoyancy}$, and drag force $\mathbf{v}_{coupling}$. The buoyancy is calculated by the following formula:

$$\mathbf{F}_{buoyancy} = m_a \cdot (-k_b^{large}\mathbf{g}) \cdot k_b^{max} - (k_b^{max} - 1) \cdot e^{-0.1N_a} \tag{13}$$

where $k_b^{large}$ is the buoyancy parameter of large-size air material, $N_a$ is the number of neighbor particles, $k_b^{max}$ is the adjustable parameter to control the max value of buoyancy force. The coupling force is:

$$\mathbf{F}_{coupling} = k_{cp}^{a\leftarrow f} \cdot A_a \cdot (\mathbf{v}_a - \hat{\mathbf{v}}_f)\|\mathbf{v}_a - \hat{\mathbf{v}}_f\| \tag{14}$$

where $k_{cp}^{a\leftarrow f} = -0.5 C_a \rho_a$ is the coupling parameter with drag coefficient $C_a = 0.2$, air density $\rho_a = 1$, $A_a = 4\pi r_a^2$ is the surface area of the large-size air material.

For large spray, $\mathbf{F}_{fluid}^{spray} = 0$. For large foam, $\mathbf{F}_{fluid}^{foam} = \mathbf{F}_{coupling}^{foam}$. For large bubble, $\mathbf{F}_{fluid}^{spray} = \mathbf{F}_{buoyancy}^{bubble} + \mathbf{F}_{coupling}^{bubble}$.

Coupling with Air Material. Air particles groups that are not in Plateau equilibrium are unstable, and will quickly be rearranged to equilibrium under surface tension. The Plateau equilibrium distance of two air particle $i$ and $j$ is $d = \sqrt{(r_i^2 + r_j^2) - \lambda \cdot r_i \cdot r_j}$, where $r_i$ and $r_j$ is the radius of these two particle respectively [7]. Since air particles with high coupling degree with fluid will surrounded by fluid particles, the equilibrium distance is different slightly. $\lambda$ is set to $-4$ for bubble particles, and is set to 1 for spray and foam particles. When the distance between two air particles are smaller than support radius, attractive force will try to pull them toward Plateau equilibrium. If two bubbles are too close than Plateau equilibrium distance, the force will turn to repulsion due to surface minimization and volume limitation.

In molecular dynamics, Lennard-Jones potential function is used to describe the interaction between two atoms. However, the initial

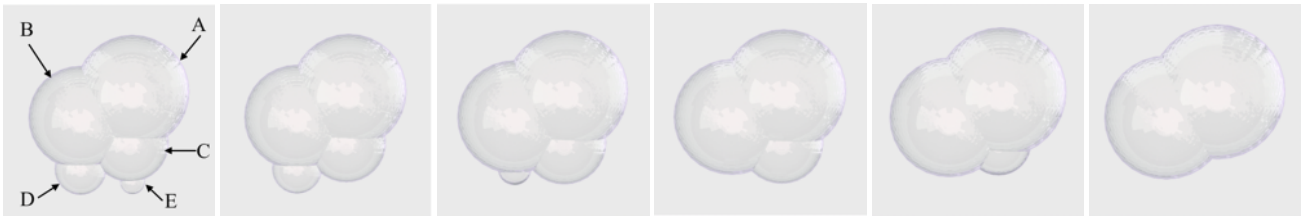


Figure 9: Five large air particles contact to each other and exchange air. The air particles with small radius tends to press air into a air particle with large radius. and five air particles are gradually merged. The radius of particle A, B, C, D, E is 0.22m, 0.2m, 0.15m, 0.1m, 0.05m, respectively. Two air particles with larger volume difference will have a more faster mass transfer speed. In the last subfigure, since the volume ratio of the two air particles is close to 0.8, the air transfer speed between them is extremely slow.

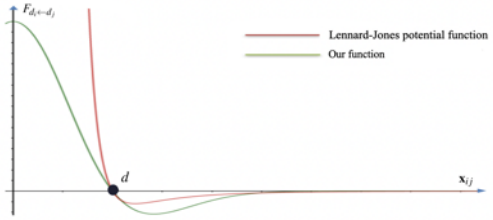


Figure 10: Lennard-Jones potential function and our new kernel function. When two air particles are too closed, the lennard-Jones potential function appears as a extremely large repulsive force, resulting in explosion effect. On the contrast, our method in more smooth in this case, and the repulsive force is much more soft.

position of air particles has a large randomness. Two closed particles will be subject to great repulsive forces, resulting in a explosion phenomenon. To solve this problem, we use a new high-order kernal function to deal with the interaction between two large air particles:

$$\mathbf{F}_{a_i \leftarrow a_j} = \mathbf{x}_{ij} \cdot k_{aa}^{max} \cdot (d^2 - {\mathbf{x}_{ij}}^2) \cdot e^{-k_{aa}^{min} \cdot {\mathbf{x}_{ij}}^2} \tag{15}$$

where $\mathbf{x}_{ij} = \mathbf{x}_i - \mathbf{x}_j$ is the distance particles $a_i$ and $a_j$, $k_{aa}^{max}$ and $k_{aa}^{min}$ are two adjustable parameter to control the maximum and minimum value of the force.

As shown in Fig. 10, it can be seen that the high-order smoothing function satisfies the property of being a repulsive force when the distance is too close. It appears as an attractive force when two particle is not that closed, and gradually weakens as the distance increases. In contrast to Lennard-Jones potential function, the peak value of our function is a finite value, thereby avoiding the explosion phenomenon.

Coupling with Solid. Some rigid bodies are hydrophilic and have an adsorption effect on the air materials. For example, when stirring the milk, the foam will adhere to the edge of the cup. Therefore, we use a pattern similar to the Eq. 15 to describe the coupling force from solid particle $s_j$ to air particle $a_i$:

$$\mathbf{F}_{a_i \leftarrow s_j} = \mathbf{x}_{ij} \cdot k_{as}^{max} \cdot (d^2 - {\mathbf{x}_{ij}}^2) \cdot e^{-k_{as}^{min} \cdot {\mathbf{x}_{ij}}^2} \tag{16}$$

where the control parameters $k_{as}^{max}$ and $k_{as}^{min}$ take different values.

Mass Transfer. According to Laplace-Young's law, the internal and external pressure difference $\Delta P$ of air material is inversely proportional to its radius $R$: $\Delta p = \frac{4\sigma}{R}$, where $\sigma$ is the surface tension coefficient. It can be seen that the pressure of small bubbles is larger than that of large bubbles. When two bubbles contact each other, the smaller one tend to press the internal air into the large one. Since the radius of the large-size air particles in this paper is not the same, air transfer phenomena can be observed.

The mass transfer process between two air particles has the following two characteristics: 1) The larger the volume ratio of the two air particles, the faster the mass transfer rate. 2) The closer the distance between the two air particles, the faster the mass transfer rate. Therefore, we describe the process of particle $a_j$ transfer air to particle $a_i$ using an inverse diffusion equation. The discretized mass transfer formula is:

$$\frac{dV_i}{dt} = \Gamma \Delta V = \Phi \sum_j V_{ij} \frac{\mathbf{x}_{ij}}{\mathbf{x}_{ij}^2 + 0.01h^2} \cdot \bigtriangledown W_{ij} \tag{17}$$

where $V_i$ is the volume of particle $i$, $\Delta$ is the Laplace operator, $\Gamma$ is the transfer coefficient. $\Phi$ is the final transfer parameter, $W_{ij}$ is smooth kernal represented by a b-spline function [25].

In order to determine whether the two air particles $a_i$ and $a_j$ will transfer air, the following decision rule is applied:

- Only two large bubbles with a large volume difference will transfer air between each other, and the threshold value is $\frac{min(V_i,V_j)}{max(V_i,V_j)} < 0.8$. This is to avoid air transfer between all bubbles, resulting in the rapidly reduced of large air materials.
- Only two bubbles in contact with each other will transfer air: $\mathbf{x}_{ij} \leq r_i + r_j$.

## 5 Experiment

In this section, we integrated our methods to a classical particle-based method, Smoothed-particle hydrodynamics (SPH method) [2], to verify the experimental results. The bullet rigid body engine is used to deal with rigid body motion.Experiments was conducted on a workstation with Intel Xeon CPU E5-2637 v4 (3.5GHz), 80GB RAM, and NVIDIA Quadro M5000 GPU.

We Use OpenGL for particle state pre-rendering, and used Blender and Cycles renderer for high-quality offline rendering. The anisotropic method [36] are used for surface reconstruction to obtain a smoother fluid surface. In the offline rendering process, the fluid is rendered as a transparent liquid using reverse ray tracing. Using the volume rendering method, the small-size air particles are rendered as white, fine particles with a rough surface based on the position. Considering the effect of underwater pressure and surface tension, large size air particles are approximately spherical. Since the volume of air materials is small, their deformation is not obvious. Therefore, large-size air particle are rendered as spherical entities with the radius calculated by Eq. 5. The precise geometric deformation is neglected, thereby reducing the calculation overhead.

### 5.1 Unified Modeling of Multiple Scale air Materials and Fluid

To verify the effectiveness of our unified modeling framework, a fluid injecting scene and two fluid-solid coupling scene was set.

Table 2: The parameters in our experiments.

| | $Q^k_{max}$ | $Q^k_{min}$ | $Q^v_{max}$ | $Q^v_{min}$ | $T$ | $k^{foam}_{cp}$ | $k^{bubble}_{cp}$ | $k^{bubble}_{b}$ | $k^{max}_{b}$ | $k^{large}_{b}$ | $k^{max}_{aa}$ | $k^{min}_{aa}$ | $k^{max}_{as}$ | $k^{min}_{as}$ | $\mu$ | $\sigma$ |
|---|---|---|---|---|---|---|---|---|---|---|---|---|---|---|---|---|
| **Fig. 1** | 9 | 0.8 | 0.6 | 0.02 | 10 | 0.4 | 0.6 | 70 | 1.9 | 1.6 | 18000 | 850 | 6500 | 90 | - | - |
| **Fig. 2** | 9 | 0.8 | 0.8 | 0.05 | 10 | 1.0 | 1.5 | 40 | 1.9 | 1.6 | 18000 | 850 | 9900 | 90 | -5.7 | 1.1 |
| **Fig. 5** | 180 | 40 | 2 | 0.5 | 5 | 0.8 | 1.0 | 5.0 | 2 | 1.5 | 2500 | 850 | 6500 | 90 | -10 | 1 |

Fluid Injecting into a Pool In Fig 1, a fluid flow was injecting into a pool. During the continuous injection of liquid, air is constantly dragged into fluid, producing a large amount of air materials. As showed in Fig 1, the small size and large size air materials (marked as red dots and blue spheres, respectively) exist simultaneously, and the large-scale air particles have different radii. The radius is calculated by Eq. 5. In this experiment, control parameters $\mu$ was adjusted to achieve different radius ranges of large air particles. It can be seen that if there is only small-scale materials (see Fig 1(b)), the visual effect is not realistic. Compared to other parameter values, $\mu = -10$ produce a better result in this scene, which is the most similar to real scene (Fig 1(a)). Under our simulation framework, animator is able to adjust the parameters as needed to achieve the desired animation effect.

Solid Body Drop into Fluid As shown in Fig 4, several blocks fall into the water, trapping air in liquid. Since the coupling degree with water is different, the motion pattern of different air materials is also different. In this experiment, different air particles are marked in different colors. Among them, the coupling degree of spray(light blue) is the lowest, followed by foam(green), and the coupling degree of bubbles(red) is the highest. It is obvious that spray is splash around, the foam is attached to the free surface, while bubbles are under the water.

As shown in Fig. 2, a dolphin falling into the sea and air is trapped in the liquid. As the interaction between dolphins and seawater deepens, the amount of diffusion material becomes larger and larger. When the tail of the dolphin swings to the right, both the fluid and the air material are affected. The trajectory of air particles can reflect the motion state inside the fluid volume, which is hard to observe without adding air materials. This experiment shows that our method can describe the interaction between air, fluid and rigid bodies realistically. After adding air materials, this scene is more vividly.

### 5.2 Detailed Experiments

The physical properties of the air materials are very complex, for example, their motion trajectory is irregular, and the interaction between the mass materials is very diverse. Therefore, our model also describes the Brownian motion and air transfer of air materials.

Brownian Motion. As shown in Fig. 5, if Brownian motion is not considered, the trajectory of the air particles will be periodic. Therefore, we implements a perturbed motion pattern by changing the angle of motion of the air material anisotropically. The animators can achieve different visual effects by adjusting the Brownian coefficient $\kappa$. In our experiment, $\kappa = 0.8$ gives the best result.

Mass Transfer As shown in Fig 9, when bubbles (large-size, high-coupled air particle) are in contact with each other, the air transfer phenomenon will occurs. Smaller bubbles will squeeze the internal air into the large bubbles due to the higher pressure. It could be seen that the bubbles disappear in order from small to large in volume. The last two bubbles have a very low air transfer rate, due to their volume ratio is closed to 0.8.

### 5.3 Parameters

All parameter value in the above experiments could be found in Tab. 2. Our method is highly controllable, different simulation effects can be achieved by adjusting all these parameters according to the animators' needs. Velocity difference parameters($Q^k_{max}$, $Q^k_{min}$) and kinetic energy parameters($Q^v_{max}$, $Q^v_{min}$) are used to control the quantity of the generated air particles according to kinetic energy and the velocity difference. Chaotic scenes tend to use larger velocity difference parameters, and fast-flow scenes tend to use larger kinetic energy parameters. We found that for scenes containing only small-sized air materials, a full frost effect can be achieved by using larger parameter value, and the simulation effect will be more realistic. $k^{bubble}_b$ is the buoyancy parameter to control the rising acceleration of small bubbles. Because air particles have a horizontal component velocity, different rising accelerations will cause different trajectories. When the ascending acceleration is large, the vertical velocity component of the air particles is larger, and the ascending trajectory is also steeper. $k^{max}_{aa}$ is used to control the maximum force between two large size air particles. With a lower value, the interaction between two air particles will be softer, and the effect of fluid particles on air particles will be greater.

### 5.4 Limitations

Our method tends to generated air particles in fast-moving areas, and the one-way coupling scheme makes it more suitable for efficient real-time simulations rather than high-accuracy simulations. In terms of deletion scheme, although we set the large size air particles with larger surface energy to be more prone to be deleted, some large size spray particles still have a long lifetime. These surviving air particles will be able to jump out of the liquid surface, affecting the visual effect of animation. This issues could, potentially, be resolved by using a smaller buoyancy parameter to reduce the velocity of these particles as they approach the surface. Fully optimizing this problem will be our future research work.

## 6 Conclusion and Discussion

In this paper, a unified simulation method for multiple-scale air materials is proposed. The air materials are generated at the area with large kinetic energy and velocity difference. Then each air particle will be assigned a type according to its size and coupling degree with fluid particles. A multiple-scale dynamics model is established to control the moving pattern of different type of air particles. By ignoring the feedback from a air particle to fluid particle, efficient one-way coupling in achieved via velocity field. Brownian motion using Schilk random function solved the problem of regular distribution of air materials. Mass transfer are described by inverse diffusion equation. The new large-size air material dynamics using our new smooth function ensures the Plateau equilibrium, achieving a realistic visual effect.


## Acknowledgments

The authors acknowledge the financial support from the National Key Research and Development Program of China (No. 2016YFB0700 500), and the National Science Foundation of China (No. 61702036, No. 61873299), and Key Research Plan of Hainan Province (No. ZDYF2018139). This work was supported by Beijing Top Discipline for Artificial Intelligent Science and Engineering, University Science and Technology Beijing.

## REFERENCES


[1] M. Akinci and M. Teschner. Animation of air bubbles with sph. 2011.

[2] M. Becker and M. Teschner. Weakly compressible SPH for free surface flows. In *Proceedings of the 2007 ACM SIGGRAPH/Eurographics symposium on Computer animation*, pp. 209–217, 2007.

[3] J. Bender and D. Koschier. Divergence-free smoothed particle hydrodynamics. In *Proceedings of the 14th ACM SIGGRAPH/Eurographics Symposium on Computer Animation*, pp. 147–155. ACM, 2015.

[4] J. Bender, D. Koschier, T. Kugelstadt, and M. Weiler. Turbulent micropolar sph fluids with foam. *IEEE transactions on visualization and computer graphics*, 25(6):2284–2295, 2018.

[5] P. Blasi, B. Le Saec, and C. Schlick. A rendering algorithm for discrete volume density objects. In *Computer Graphics Forum*, vol. 12, pp. 201–210. Wiley Online Library, 1993.

[6] R. Bridson. Fluid simulation for computer graphics. *A K Peters*, 2008.

[7] O. Busaryev, T. K. Dey, H. Wang, and Z. Ren. Animating bubble interactions in a liquid foam. *ACM Transactions on Graphics (TOG)*, 31(4):63, 2012.

[8] N. Chentanez and M. Müller. Real-time eulerian water simulation using a restricted tall cell grid. In *ACM Transactions on Graphics (TOG)*, vol. 30, p. 82. ACM, 2011.

[9] P. W. Cleary, S. H. Pyo, M. Prakash, and B. K. Koo. Bubbling and frothing liquids. In *ACM Transactions on Graphics (TOG)*, vol. 26, p. 97. ACM, 2007.

[10] C. Gissler, S. Band, A. Peer, M. Ihmsen, and M. Teschner. Approximate air-fluid interactions for sph. In *VRIPHYS*, pp. 29–38, 2017.

[11] Y. Gu and Y.-H. Yang. Physics based boiling bubble simulation. In *SIGGRAPH ASIA 2016 Technical Briefs*, p. 5. ACM, 2016.

[12] N. Hassan, M. M. K. Khan, M. Rasul, et al. A study of bubble trajectory and drag co-efficient in water and non-newtonian fluids. *WSEAS Transactions on Fluid Mechanics*, 3(261):e270, 2008.

[13] J.-M. Hong, H.-Y. Lee, J.-C. Yoon, and C.-H. Kim. Bubbles alive. *ACM Transactions on Graphics (TOG)*, 27(3):48, 2008.

[14] M. Ihmsen, N. Akinci, G. Akinci, and M. Teschner. Unified spray, foam and air bubbles for particle-based fluids. *The Visual Computer*, 28(6-8):669–677, 2012.

[15] M. Ihmsen, J. Orthmann, B. Solenthaler, A. Kolb, and M. Teschner. SPH fluids in computer graphics. In *Eurographics 2014: STARs*, 2014.

[16] D. Kim, O.-y. Song, and H.-S. Ko. A practical simulation of dispersed bubble flow. In *ACM Transactions on Graphics (TOG)*, vol. 29, p. 70. ACM, 2010.

[17] J.-H. Kim, W. Kim, and J. Lee. Physics-inspired approach to realistic and stable water spray with narrowband air particles. *The Visual Computer*, 34(4):461–471, 2018.

[18] J.-H. Kim, J. Lee, S. Cha, and C.-H. Kim. Efficient representation of detailed foam waves by incorporating projective space. *IEEE transactions on visualization and computer graphics*, 23(9):2056–2068, 2016.

[19] T. Kim and M. Carlson. A simple boiling module. In *Proceedings of the 2007 ACM SIGGRAPH/Eurographics symposium on Computer animation*, pp. 27–34. Eurographics Association, 2007.

[20] D. Koschier, J. Bender, B. Solenthaler, and M. Teschner. Smoothed particle hydrodynamics techniques for the physics based simulation of fluids and solids. 2019.

[21] Z. Li and S. Xiao. Boiling simulation of position based fluid. In *Proceedings of the 4th International Conference on Virtual Reality*, pp. 142–146. ACM, 2018.

[22] A. Matsuura and L.-S. Fan. Distribution of bubble properties in a gas-liquid-solid fluidized bed. *AICHE journal*, 30(6):894–903, 1984.

[23] V. Mihalef, B. Unlusu, D. Metaxas, M. Sussman, and M. Y. Hussaini. Physics based boiling simulation. In *Proceedings of the 2006 ACM SIGGRAPH/Eurographics symposium on Computer animation*, pp. 317–324. Eurographics Association, 2006.

[24] J. Monaghan. Particle methods for hydrodynamics. *Computer Physics Reports*, 3(2):71–124, 1985.

[25] J. J. Monaghan. Smoothed particle hydrodynamics. *Annual review of astronomy and astrophysics*, 30(1):543–574, 1992.

[26] M. Müller, D. Charypar, and M. Gross. Particle-based fluid simulation for interactive applications. In *Proceedings of the 2003 ACM SIGGRAPH/Eurographics symposium on Computer animation*, pp. 154–159, 2003.

[27] M. Müller, B. Solenthaler, R. Keiser, and M. Gross. Particle-based fluid-fluid interaction. In *Proceedings of the 2005 ACM SIGGRAPH/Eurographics symposium on Computer animation*, pp. 237–244. ACM, 2005.

[28] J. Onderik, M. Chládek, and R. Ďurikovič. Sph with small scale details and improved surface reconstruction. In *Proceedings of the 27th Spring Conference on Computer Graphics*, pp. 29–36. ACM, 2011.

[29] M. Prakash, P. W. Cleary, S. H. Pyo, and F. Woolard. A new approach to boiling simulation using a discrete particle based method. *Computers & Graphics*, 53:118–126, 2015.

[30] B. Ren, Y. Jiang, C. Li, and M. C. Lin. A simple approach for bubble modelling from multiphase fluid simulation. *Computational Visual Media*, 1(2):171–181, 2015.

[31] X. Shao, Z. Zhou, and W. Wu. Particle-based simulation of bubbles in water–solid interaction. *Computer Animation and Virtual Worlds*, 23(5):477–487, 2012.

[32] J. Stam. Stable fluids. *ACM Transactions on Graphics*, pp. 121–128, 1999.

[33] T. Takahashi, H. Fujii, A. Kunimatsu, K. Hiwada, T. Saito, K. Tanaka, and H. Ueki. Realistic animation of fluid with splash and foam. In *Computer Graphics Forum*, vol. 22, pp. 391–400. Wiley Online Library, 2003.

[34] J. Tan and X. Yang. Physically-based fluid animation: A survey. *Science in China Series F: Information Sciences*, 52(5):723–740, 2009.

[35] N. Thuerey, F. Sadlo, S. Schirm, M. Müller-Fischer, and M. Gross. Real-time simulations of bubbles and foam within a shallow water framework. In *Proceedings of the 2007 ACM SIGGRAPH/Eurographics symposium on Computer animation*, pp. 191–198. Eurographics Association, 2007.

[36] X. Wang, X. Ban, X. Liu, Y. Zhang, and L. Wang. Efficient extracting surfaces approach employing anisotropic kernels for sph fluids. *Journal of Visualization*, 19(2):301–317, 2016.

[37] X. Xiao, S. Zhang, and X. Yang. Real-time high-quality surface rendering for large scale particle-based fluids. In *Proceedings of the 21st ACM siggraph symposium on interactive 3D graphics and games*, p. 12. ACM, 2017.

[38] X. Xiao, Y. Zhou, H. Wang, and X. Yang. A novel cnn-based poisson solver for fluid simulation. *IEEE transactions on visualization and computer graphics*, 2018.

[39] Y. Yang and X. Yang. Shape conservation of fft-based smoke simulation. In *2015 4th International Conference on Computer Science and Network Technology (ICCSNT)*, vol. 1, pp. 1478–1481. IEEE, 2015.